Acoustics of a Supersonic Mach 1.4 Axisymmetric Spike Inlet

David B. Stephens[1] and Edmane Envia[2]
NASA Glenn Research Center, Cleveland, OH, 44135, USA

An engine inlet for a supersonic commercial aircraft is analyzed for noise radiation in low-speed configurations for which auxiliary inlet doors are open. Duct modes generated by the fan are estimated by post-processing unsteady Reynold averaged Navier-Stokes (URANS) simulations of the fan and are used as boundary conditions to the inlet domain. Far-field inlet radiated tone levels are computed using commercial acoustics finite element software. The results indicated that the inlet tone levels at cutback and sideline conditions are higher by more than 20 dB than the approach levels.

I. Introduction

In 2020, NASA collaborated with GE Aviation to deliver a fan and inlet design for a supersonic commercial passenger aircraft. NASA provided the SUPIN [1] inlet design tool and provided guidance on its use. The result was an axisymmetric spike inlet designed for Mach 1.4 operation at 50,000 ft altitude. The axisymmetric and on-design geometry was modified to meet other requirements. Mechanical features were added, such as struts to hold the spike in place. The center spike was tapered to zero thickness, such that the duct geometry transitions from annular to circular upstream of the engine. For low-speed operation, an axisymmetric auxiliary inlet was added by splitting the outer cowl and translating the upstream portion forward. Actuators were added to the geometry to support the translating cowl. The resulting inlet geometry is shown in Figure 1.

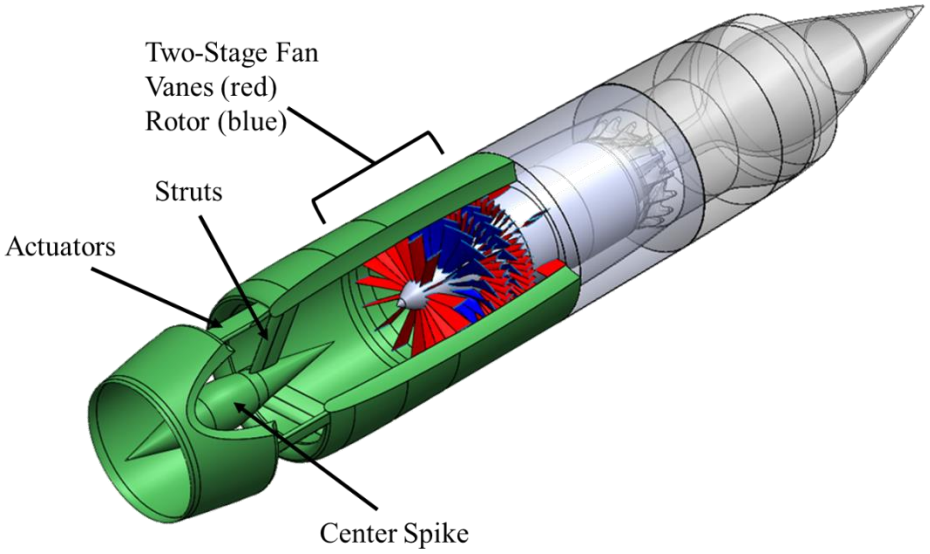

Figure 1 Inlet design used in this study.

[1] Research Engineer, Acoustics Branch, AIAA Lifetime Member.
[2] Research Engineer, Acoustics Branch, AIAA Associate Fellow.

II. Background

A similar axisymmetric spike inlet was used in a NASA Glenn Research Center study [2] of the Low-Boom Flight Demonstrator, although a simpler pitot inlet was chosen for use on the X-59 aircraft [3]. The axisymmetric spike inlet study concluded that the appropriate flight speed for transitioning between open and closed auxiliary inlet configurations was Mach 0.6. This flight speed is well above the 250 knot noise certification speed limit specified in FAR 36 [4], so the relevant configuration for acoustic analysis is with the auxiliary inlet open. Studies on the acoustics of a representative supersonic passenger jet suggested that fan noise at approach condition is likely to be a major contributor to the overall certification noise level of a commercial supersonic aircraft [5], further motivating the present work.

The NASA Commercial Supersonics Technology (CST) project sponsored a study by GE Aviation, Lockheed Martin and Stanford University [6] that developed a concept vehicle called the LM1044, a Mach 1.7, 80-passenger tri-jet. This concept vehicle also utilized an axisymmetric spike inlet with a translating cowl auxiliary inlet. The design of this engine inlet included details such as struts and cowl support actuators, similar to the present geometry. As described in Section 7.2 of [6], a linearized Navier-Stokes code was used for CAA to study noise propagation through the inlet, auxiliary doors and consider the presence of struts. A few observations were made, such as the auxiliary opening being a significant noise leakage path. The study also concluded that the auxiliary inlet will be open at noise certification.

The F120 fan model [7] was developed during the NASA High Speed Research (HSR) program and is based on test data from a single engine with a three-stage fan tested on a stand with a bellmouth inlet. As part of the HSR program, research was conducted into the effect of inlet geometry on the fan noise. This included several studies at Virginia Tech ([8] and [9]) and an investigation at the Boeing Low-Speed Aero-acoustic Facility (LSAF) [7] which was used to develop a correction for a two-dimensional (2D) bifurcated inlet. Discussion in the report is brief, but the corrections are rather elaborate, giving a frequency- and directivity-dependent curve for broadband noise. Four corrections are available, for the three aircraft noise rating conditions of sideline, approach, and flyover, also called centerline. The centerline correction is provided both with the auxiliary inlet doors open and closed. The disposition of the doors for the other two cases is not clear. Since these corrections were developed with a fan model, they include the effect of the inlet geometry combined with the resulting flow distortion on the fan source.

The present paper presents a workflow previously demonstrated for subsonic fan tone noise prediction [10] starting with the estimated tone levels generated by the fan. Though the inlet and fan geometry are vastly different for the supersonic case, the same physics based models apply within the limits of the assumptions made in the workflow. The method uses high-resolution unsteady Reynolds averaged Navier-Stokes simulations of the fan stage unsteady flow from which acoustic model content are extracted and fed as input to inlet radiation simulations. The principal mechanism of noise generation modeled using this approach is the blade row interactions which include both the viscous and potential interactions. The present paper is focused on inlet radiated noise only, though the workflow is equally applicable to the exhaust noise. Also, only fan tone is considered in this study.

III. Geometry

For the purposes of this study, the supersonic inlet shown in green in Figure 1 was used in combination with a two stage fan. This fan-inlet combination is a preliminary design that includes the principal expected features of a supersonic engine and represents a good starting point for acoustic analysis.

A. Inlet Simplification

As a preliminary step, the 3-D inlet was converted to a 2-D axisymmetric version with the struts and cowl supports removed. A fluid volume was added around the geometry where finite element analysis will be conducted. Such 2-D inlet representations are commonly used for acoustic simulations for subsonic inlet geometries, are quick to run and can cover the entire frequency range of interest. This simplified inlet is shown in **Error! Reference source not found.**. Comparisons for similar geometry inlets in 2-D vs 3-D will be part of a future analysis.

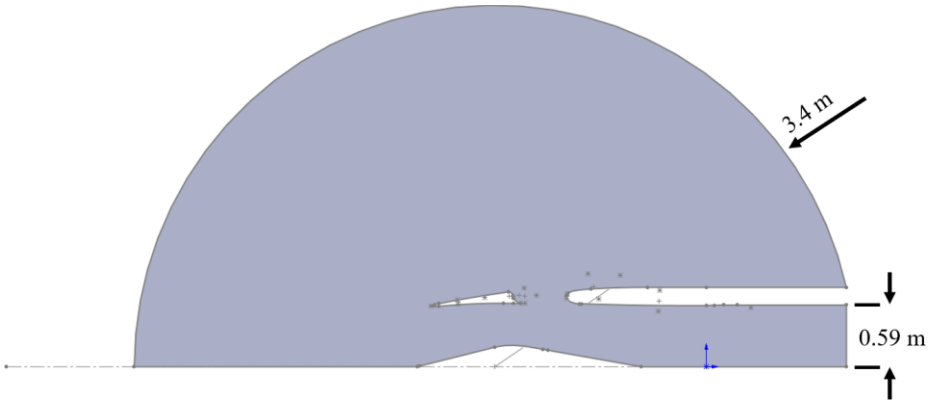

Figure 2 Two-dimensional inlet representation.

B. Two-Stage Fan

The trend in fans for subsonic aircraft has been towards large fan diameters, lower pressure ratios, higher bypass ratios, shorter inlets, and lower blade counts. All of these trends are in contrast to those for the supersonic aircraft fan design. For supersonic applications, the engine needs to be slender to reduce drag. As such, the pressure ratio is necessarily large. The bypass ratio is also lower than that for a subsonic turbofan. The inlet must be long to efficiently decelerate the airflow before reaching the fan face. Furthermore, the two-stage design typically necessitates inlet guide vanes for condition the flow ingested by the fan. The present two-stage fan design is shown in schematic in Figure 3.

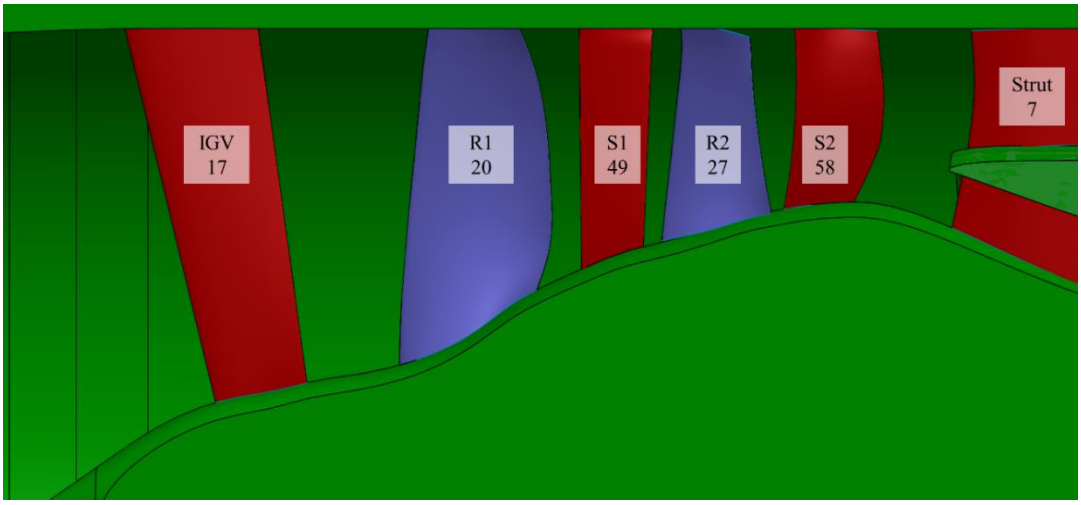

Figure 3 Flow path and blade counts for two-stage fan. Rotating blades colored blue.

Operating conditions for the fan at noise certification points were also delivered. These are summarized in Table 1. These will be used to set operating conditions for the engine during simulation and for the flow field used in the acoustic analysis.

Table 1 Two-Stage Fan Conditions

	Approach	Cutback	Sideline	Takeoff
Flight Speed (m/s)	90	121	123	88
Fan Face Speed (m/s)	107	140	173	194
RPM	4533	5733	6672	7200
First Stage Fan BPF, Hz	1511	1911	2224	2400

C. Modal Content

A two-stage fan is expected to produce a richer azimuthal mode content (i.e., Tyler-Sofrin modes) than a single-stage fan. This requires the simulation of multiple azimuthal mode orders during geometry evaluation. The Actran [9] utility *cutget* was used to compute the cut-on frequencies for a circular duct, radius 0.5867 m (23.1 inch) with an axial velocity of 150 m/s. The results for the lowest order radial (designated $n = 0$ in the present paper) are shown in Figure 4. A linear fit shows that azimuthal modes cut on approximately every 84 Hz, starting at 100 Hz. This is a convenient rule of thumb for this specific inlet when considering whether a specific azimuthal mode order is going propagating or evanescent.

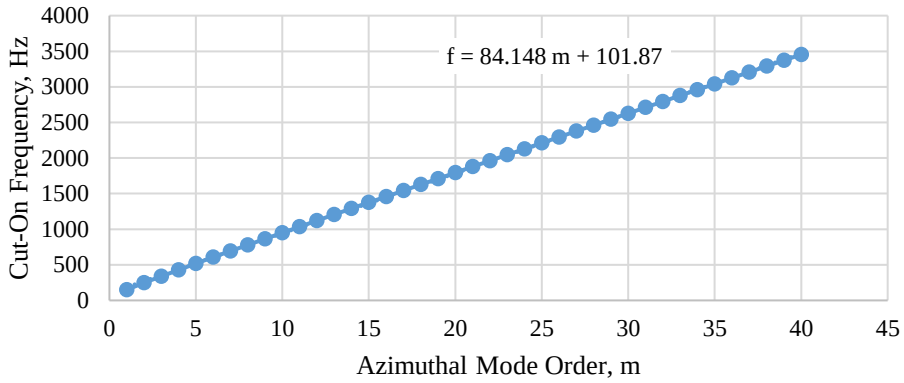

Figure 4 Azimuthal mode cut on frequencies at interface plane to inlet

The Tyler-Sofrin mode counts for the first 1.5 fan stages are given in Table 2 and 3 for IGV/blade/vane counts of 17/20/49. The fan shaft speed at approach was used to calculate the relevant blade passing frequencies. The first blade passing tone has a frequency of 1550 Hz and is cut-off by the duct geometry and should not propagate. The highlighted cells of the tables show the likely propagating candidates. For the Rotor 1 interacting with Stator 1, which is the typical source for conventional subsonic fans, the azimuthal modal content are $m = -9$ at the second blade passing tone (at 3100 Hz) and $m = 11$ for the third blade rate tone (at 4650 Hz). Note that negative values of the index k are also possible but for these blade counts they generate mode orders m that are too high to propagate.

Table 2 Tyler-Sofrin mode numbers for IGV / Rotor 1 interaction
(note: highlighted cells indicate cut-on modes)

$m = n\,N_B - k\,N_V$		1550 Hz	3100 Hz	4650 Hz	6200 Hz	7750 Hz
N_B=20		Harmonic in static frame (n)				
N_V=17		1xBPF	2xBPF	3xBPF	4xBPF	5xBPF
Harmonic in rotating frame (k)	0	20	40	60	80	100
	1	3	23	43	63	83
	2	-14	6	26	46	66
	3	-31	-11	9	29	49
	4	-48	-28	-8	12	32

Table 3 Tyler-Sofrin mode numbers for Rotor 1 / Stator 1 interaction
(note: highlighted cells indicate cut-on modes)

$m = n\,N_B - k\,N_V$		1550 Hz	3100 Hz	4650 Hz	6200 Hz	7750 Hz
N_B=20		Harmonic in static frame (n)				
N_V=49		1xBPF	2xBPF	3xBPF	4xBPF	5xBPF
Harmonic in rotating frame (k)	0	20	40	60	80	100
	1	-29	-9	11	31	51
	2	-78	-58	-38	-18	2
	3	-127	-107	-87	-67	-47
	4	-176	-156	-136	-116	-96

IV. Simulations

The workflow for computing the inlet radiation tone levels includes three major steps: A turbomachinery unsteady aerodynamic simulation for the fan stages, an inlet flow simulation in a free field, and an acoustic radiation simulation. The following sections describe an overview of the individual steps.

A. Unsteady RANS

High-resolution simulations of the two-stage fan were carried out using the FINE™/Turbo CFD software [12]. The advantageous aspect of this tool for the present work is the capability for a selective frequency-domain URANS simulation approach called the non-linear harmonic (NLH) method. This approach tracks a pre-selected number of BPF harmonics for each blade rows and requires only a single passage of each blade row to be included in the computations. The computational domain used for the NLH simulations is shown in Figure 5.

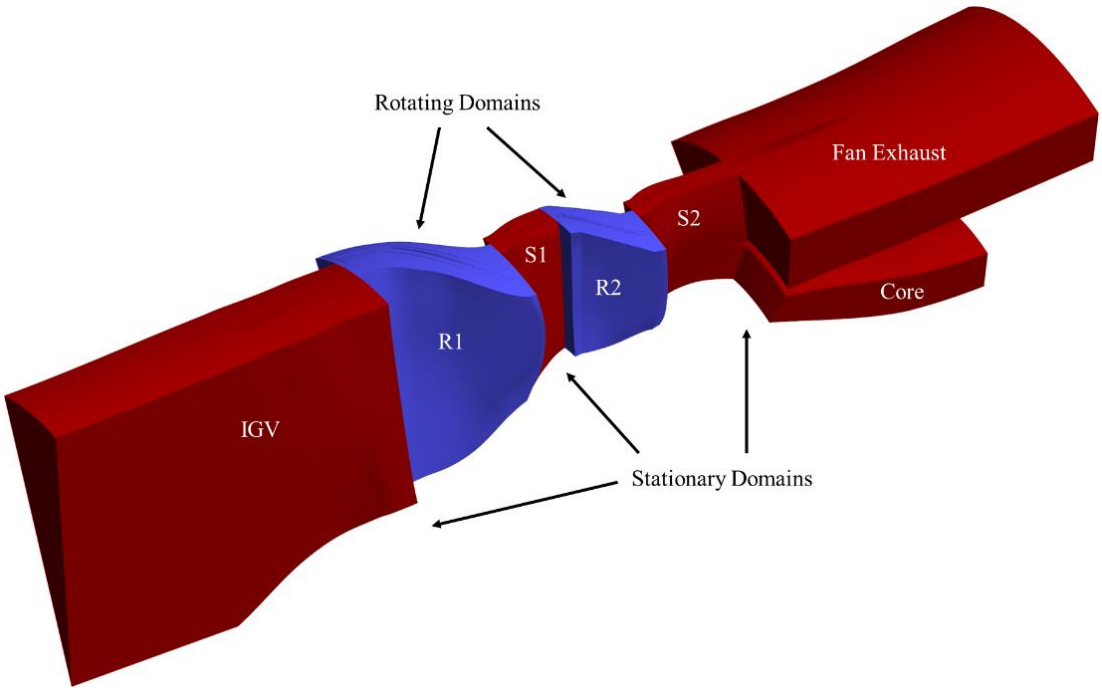

Figure 5 Domain used for URANS, rotating in blue, stationary in red

The NLH simulations were post-processed using the Actran iTM package to create a full-wheel axial plane of pressure and velocity components upstream of the spinner. This is the interface plane used between the URANS and acoustic simulations used in this work. The result for the perturbations at the BPF tone at the approach condition is shown in Figure 6.

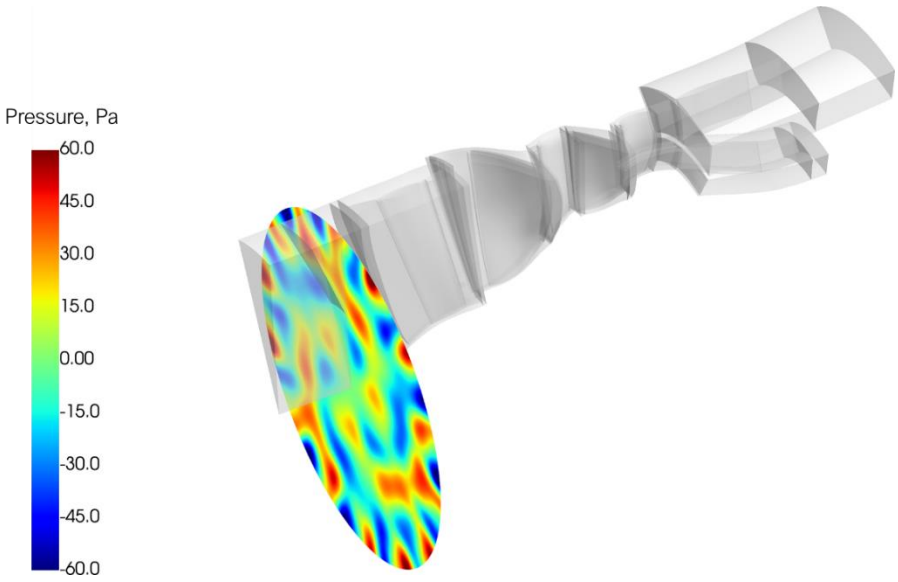

Figure 6 Real part of frequency domain peak-to-peak complex pressure on the plane used for computing duct mode amplitudes (1xBPF=1550 Hz, Ω=75.6 Hz)

Results for the four operating conditions investigated in this paper are shown in Figure 7. The principal mode orders making up each of the pressure maps are the largely the same, but the levels of the resulting tones are dramatically different, e.g., approach = 77 Pa (132 dB), cutback = 1710 Pa (159 dB), sideline = 1059 Pa (154 dB) and takeoff = 352 Pa (145 dB).

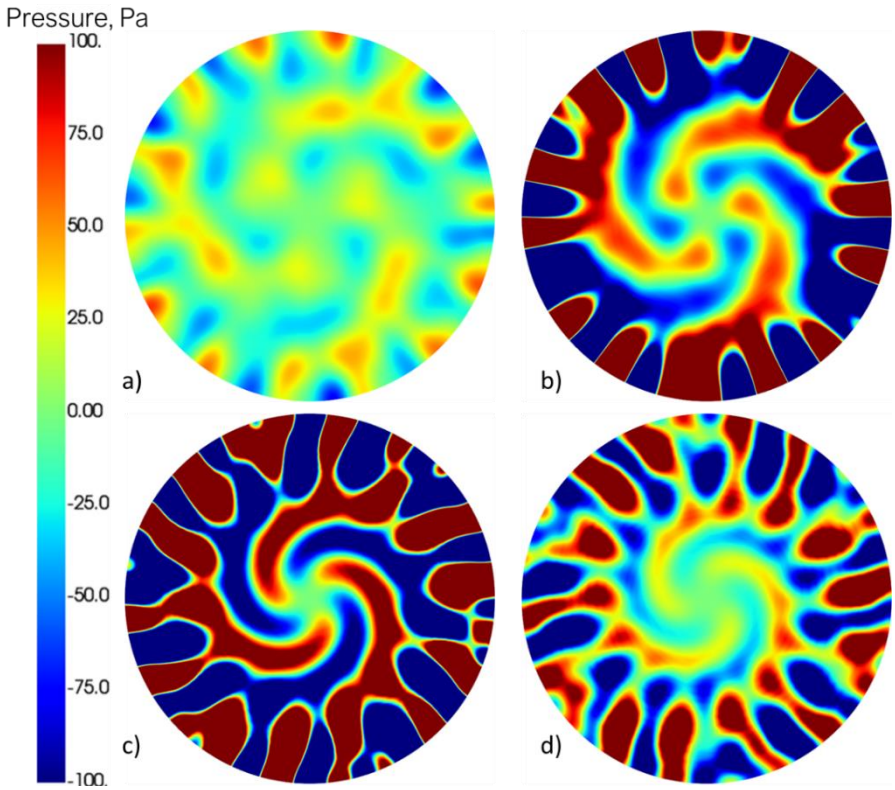

Figure 7 Real part of frequency domain peak-to-peak complex pressure at 1x BPF for a) approach, b) cutback, c) sideline, d) takeoff. Shaft speeds as indicated in Table 1.

The Actran iTM tool fits analytical duct mode shapes to the unsteady pressure perturbation field extracted from the URANS simulation. An example is shown in Figure 8, for the case of approach fan speed for 1xBPF. The output of iTM includes the radial content but for the sake of this example, these were summed together to give a combined amplitude for each azimuthal mode order considered. Comparing the modal content to Table 2, it is clear that all the major interaction orders are accounted for in the simulation. The m = 3 and m = -14 modes are the dominant cut-on modes, being the lowest. Mode orders in the 2xBPF tone include m = 6 and m = -11. Some additional content is observed, likely due to aliasing or scattering.

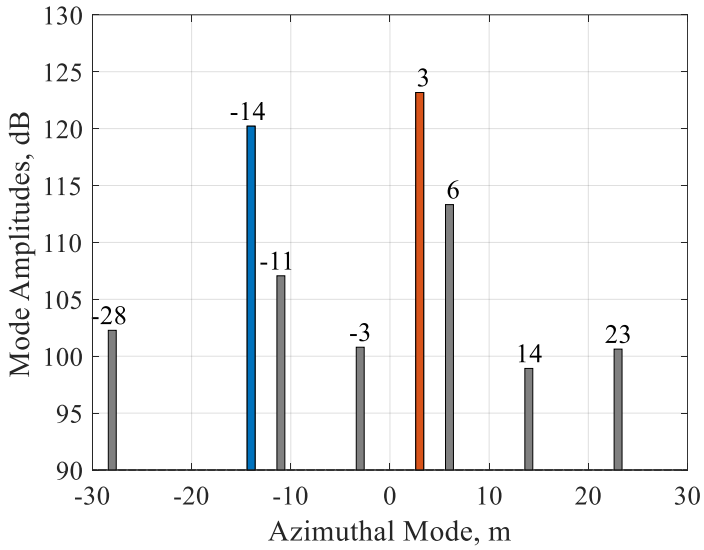

Figure 8 Approach 1xBPF sum of radial mode amplitudes

The output of Actran iTM is a table of azimuthal and radial mode complex amplitudes, of which there can be hundreds for the frequency and geometry of interest. The most significant mode amplitudes are the m = -14 and m = 3, which each are presented in Figure 8 as the sum of radial modes. As an example, the individual radial mode amplitudes for these two azimuthal modes are presented in Figure 9. The strongest single mode is the (-14,0) mode, at 120 dB, observed in both Figure 8 and Figure 9. The results for the other fan operating conditions are omitted from the present report for the sake of brevity.

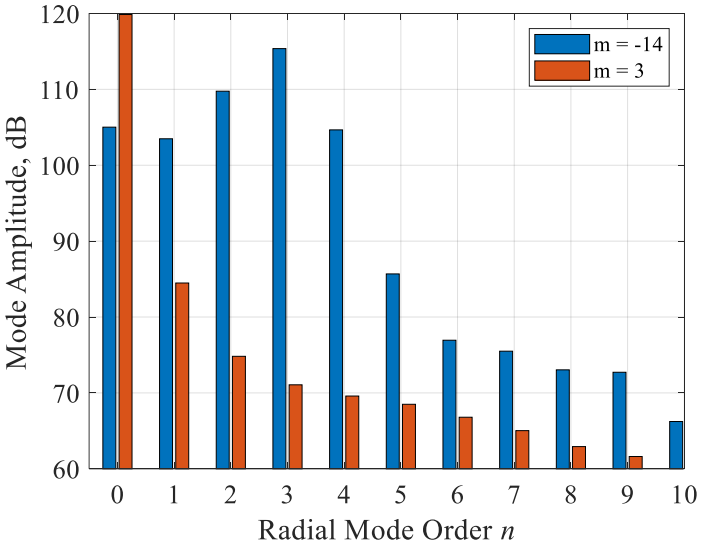

Figure 9 Upstream propagating radial mode amplitudes for approach condition

As Figure 8 makes clear, however, most of the amplitudes are tens of decibles below the main modal peaks. The output from processing the four URANS simulations for the upstream propagating tone noise are shown in Figure 10. The amplitudes at the approach condition are seen to be the lowest, some 20 dB below those for cutback and sideline. The takeoff levels are lower than those for cutback and sideline and about 10 dB above those for the approach condition. Note that each of these azimuthal mode amplitudes presented here is a sum of the constituent radial mode amplitudes not presented in detail here for brevity.

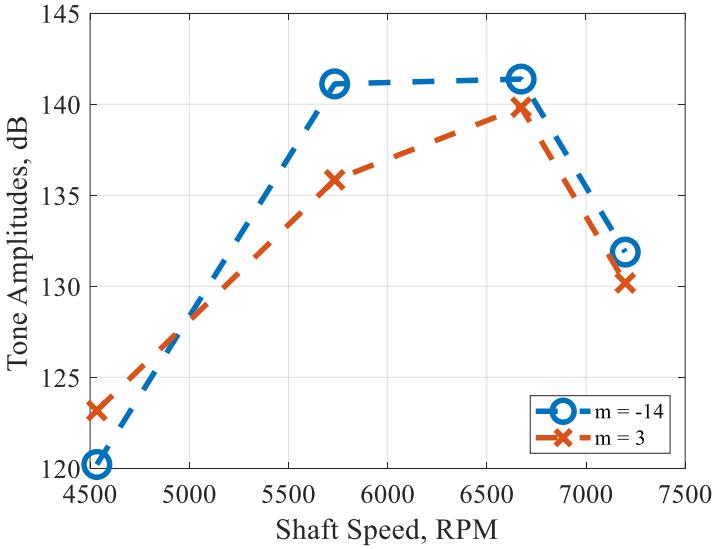

Figure 10 Tone amplitudes for four operating conditions shown in Table 1, two duct azimuthal modes

B. Inlet Flow Simulations

A set of flow simulations were conducted for the 2-D axisymmetric inlet geometry to create the necessary background flow for the acoustic simulations. The Actran compressible potential flow solver was used for that purpose and results are shown in Figure 11. Since the solver is inviscid, viscous boundary layers are not developed. The upstream cowl also does not develop a wake. A future effort will consider the effect of a more realistic, viscous, flow field.

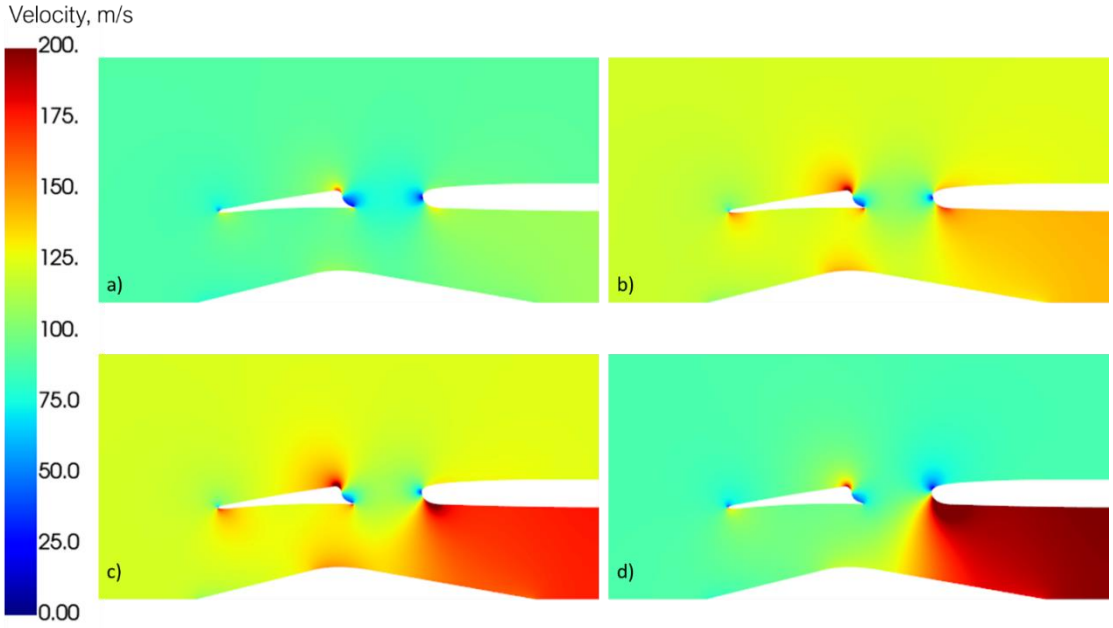

Figure 11 Flow solutions for a) approach, b) cutback, c) sideline, d) takeoff.

C. Acoustic Simulations

Acoustic simulations presented here were conducted using Actran 2022 [10] employing the Actran TM turbomachinery workflow. The 2-D inlet geometry was wrapped in a semi-circular domain of 3.4 m (135 inch) radius, centered on the mid-point between the front inlet and auxiliary inlet. This domain topology was chosen as providing a largely reflection-free computational domain when using the infinite element boundary condition. A quadratic grid with element size of 8 mm (0.315 inches) gives 4 points per convected wavelength up to the frequency of about 4500 Hz, depending on the local flow speed. This results in approximately 550,000 elements and solution times on the order of a minute per frequency on a laptop. An arc of virtual microphones at 46 m (150 ft) gives the sound radiation in the far field. Actran uses an *infinite element* method to model the sound radiation from the finite element domain through a uniform medium to the specified field points. For the present simulations, these virtual microphones are in a flow convecting with the flight speed of the inlet. The layout is shown in Figure 12.

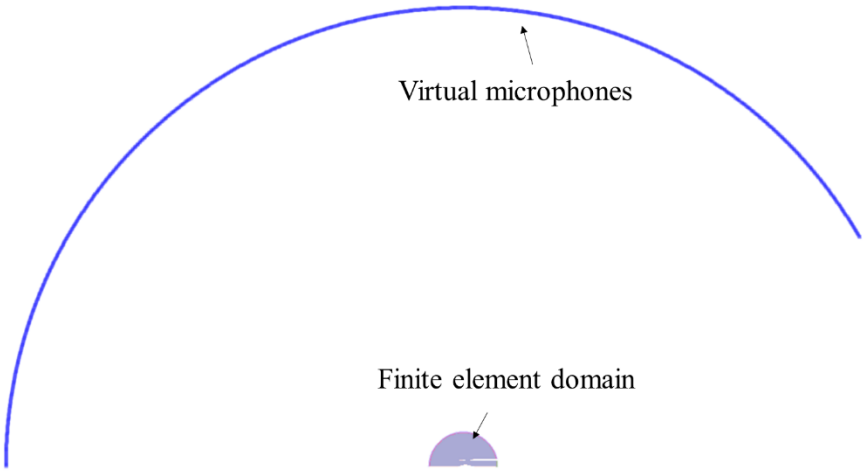

Figure 12 Actran computational domain

The acoustic content extracted from the URANS simulations using the Actran iTM tool, can now be used as the modal input (i.e., boundary condition) at the fan face. The corresponding radiation simulations provide a series of sound maps like that shown in Figure 13. In this case, the real part of the pressure is plotted with 11 input radial modes included simultaneously and with their respective phase preserved.

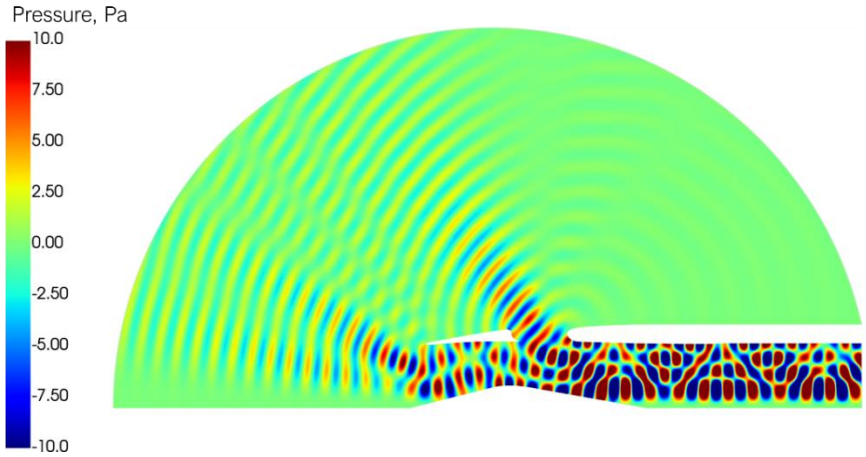

Figure 13 Real part of frequency domain peak-to-peak complex pressure for approach conditions, *m* = 3

The higher mode orders (such as m = -14) have correspondingly fewer radials (shown in Figure 9) and also propagate at a steeper angle relative to the symmetry axis of the inlet. The m = -14 mode principally propagates out of the auxiliary inlet.

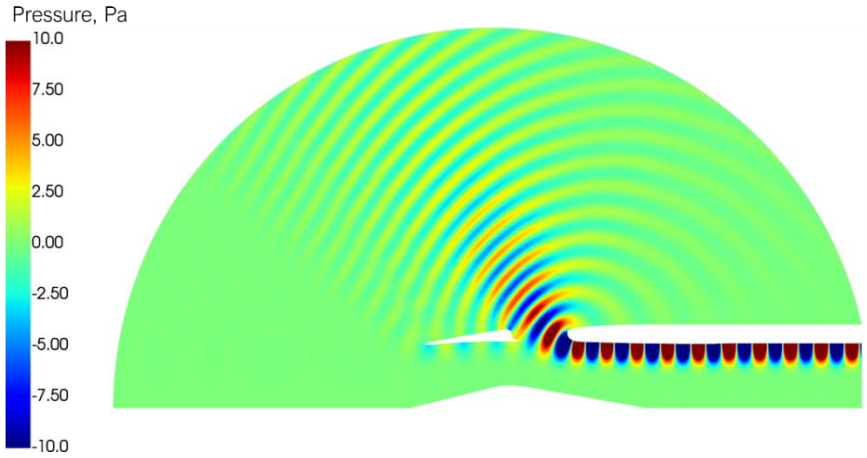

Figure 14 Real part of frequency domain peak-to-peak complex pressure for approach conditions, *m* = -14

The far field levels for the four operating conditions considered here are shown in Figure 15. For each condition, the upstream radiated noise (along the axis and near 0 degrees) is dominated by the $m = 3$ contribution. At approach, the radiated sound peaks at an angle of 50 degrees and at an amplitude of 80 dB. At cutback and sideline conditions, the levels are approximately 20 dB higher and more forward-radiated. Inlet levels for all conditions fall off rapidly for angles past 90 degrees. These predictions can be used in system noise analyses where an aircraft trajectory is used to predict sound observed by a receiver on the ground.

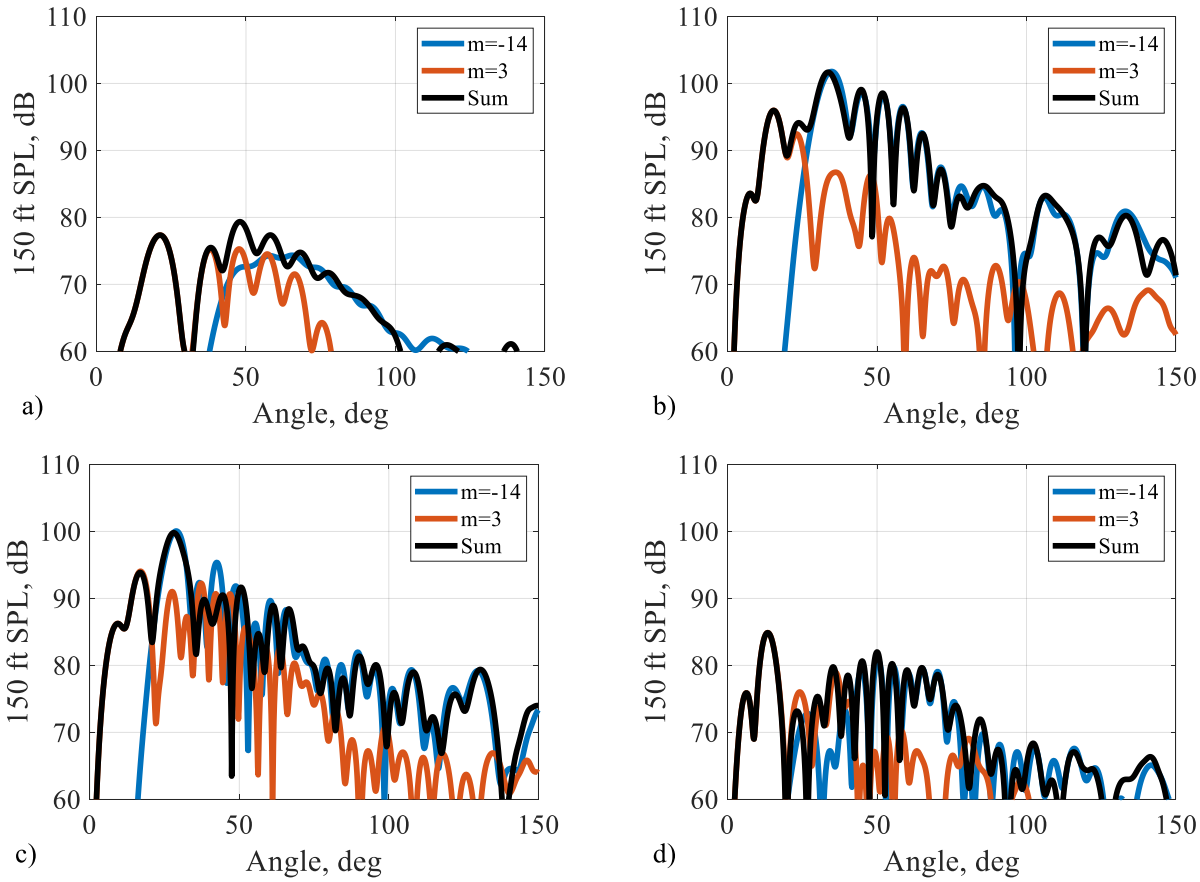

Figure 15 Far field sound predicted for a) approach, b) cutback, c) sideline and d) takeoff conditions

V. Conclusions

Inlet tone levels for a two-stage supersonic fan were predicted using physics-based simulations. The workflow presented here relies on commercial software that have been used extensively by industry and previously demonstrated by the authors to provide quite reasonable agreement with the experimental data for a subsonic fan noise. The method is computationally efficient and flexible with regards to geometry and operating conditions.

The inlet tone levels at the four operating conditions show sensitive dependance on the fan speed, with maximum levels predicted at the cutback and sideline operating conditions. The higher (takeoff) and lower (approach) fan speed conditions are considerably quieter. This is likely due to stronger fan and guide vane wakes and stronger potential field coupling. Future work will consider the effect of inlet three-dimensionality on the radiated noise, specifically the effect of the struts and inlet angle-of-attack to the freestream. It is expected that these would cause inflow distortions into the fan disc and a complicated flow field for the sound to propagate through. Additionally, complicated features of the simulated sound field including interactions and mode scattering will be further investigated.

References

[1] J. W. Slater, "SUPIN: A Computational Tool for Supersonic Inlet Design," in *SciTech Forum*, San Diego, California, USA, 2016.

[2] C. M. Heath, J. A. Seidel and S. K. Rallabhandi, "Viscous Aerodynamic Shape Optimization with Installed Propulsion Effects," in *AVIATION Forum*, Denver, Colorado, USA, 2017.

[3] V. F. Dippold, "High Speed Inlet Distortion Test for the X 59 Low Boom Flight Demonstrator in the NASA Glenn 8-by 6-Foot Supersonic Wind Tunnel," NASA TM-20220010443, July 2022.

[4] Federal Aviation Advisory Circular 36-4C, Title 14, Chap. 1, Part 36, "Noise Standards: Aircraft Type and Airworthiness Certification," U.S. Code of Federal Regulations, 2003.

[5] J. J. Berton, D. L. Huff, K. Geiselhart and J. Seidel, "Supersonic Technology Concept Aeroplanes for Environmental Studies," in *AIAA Scitech Forum*, Orlando, Florida, USA, 6-10 January 2020.

[6] J. Morgenstern, M. Bounamo, J. Yao, M. Murugappan, U. Paliath, L. Cheung, I. Malcevic, K. Ramakrishman, N. Pastouchenko, T. Wood, S. Martens, P. Viars, T. Tersmette, J. Lee and G. Carrier, "NASA/CR—2015-218719," *Advanced Concept Studies for Supersonic Commercial Transports Entering Service in the 2018-2020 Period Phase 2*, pp. 1-30, 2015.

[7] J. W. Rawls and J. C. Yeager, "High Speed Research Noise Prediction Code (HSRNOISE) User's and Theoretical Manual," NASA-CR-2004-213014, November 2004.

[8] W. Ng, "Comparison of the Aeroacoustics of Two Small-Scale Supersonic Inlets," NASA CR-96-206507, January 1996.

[9] S.-M. Li, C. A. Hanuska and W. Ng, "An experimental investigation of the aeroacoustics of a two-dimensional bifurcated supersonic inlet," *Journal of sound and vibration*, vol. 248, no. 1, pp. 105-121, 2001.

[10] A. A. Svetgoff, D. Stephens and E. Envia, "Inlet Radiated Noise Predictions for the NASA Source Diagnostic Test Fan Using Physics-Based Simulations," in *28th AIAA/CEAS Aeroacoustics 2022 Conference*, Southampton, UK, June 14-17, 2022.

[11] F. F. T. SA, "ACTRAN 2022 User's Guide," MSC Software, Mont-Saint-Guibert, Belgium, 2022.

[12] Cadence Design Systems, Inc., "FINE/Turbo Manual," San Jose, California, USA, 2022.

[13] E. Envia, "Open Rotor Aeroacoustic Modelling," NASA/TM-2012-217740, 2012.